A THREE YEAR GLOBAL INTERCOMPARISON OF ERS-1 SAR WAVE MODE SPECTRAL RETRIEVALS WITH WAM MODEL DATA

P. Heimbach, S. Hasselmann and K. Hasselmann

Max-Planck-Institut für Meteorologie, Bundesstraße 55, D-20146 Hamburg, Germany
Phon: + 49 / 40 / 4 11 73 - 3 77, Facs: + 49 / 40 / 4 11 73 - 2 98
e-mail: heimbach@dkrz.de

Abstract

A global statistical intercomparison was carried out for the period January 1993 to December 1995 between wave spectra retrieved from ERS-1 SAR Wave Mode (SWM) data using an inversion algorithm of the closed nonlinear wave-to-SAR spectral mapping relation and wave spectra computed with the wave model WAM. A combined quality analysis of the satellite data and a performance analysis of the retrieval algorithm was carried out. The assessment yielded about 75 percent successful retrievals. Time series of significant wave heights in different parts of the world oceans showed good overall agreement. However, a more detailed investigation exploring the distinct spectral properties of the windsea and swell content of the wave spectra revealed a small but systematic model overprediction of windsea and an underprediction of swell systems while the overpredicted windsea can be attributed to incorrect wind fields, the underpredicted swell could be caused by deficiencies in the model.

Keywords: ocean waves; ERS-1 SAR Wave Mode; spectral retrieval algorithm; WAM model; global statistics; partitionings of windsea and swell.

1. INTRODUCTION

One of the major goals for the first European Remote Sensing Satellite ERS-1, launched on 17 July 1991, was to obtain global wind and wave data in near real time for wave research and operational wave forecasting. A particularly useful feature of the ERS-1 microwave instrument is the SAR intermittent imaging mode (so-called "wave mode"). This provides global two-dimensional wave spectral image data derived from 5 × 10 km imagettes observed every 200 km along the satellite track (for a detailed description see Appendix A1 of [*Heimbach et al.*, 1997]). The image spectra can be converted to wave spectral data, which can then be used to validate global wave models and improve wave forecast through wave data assimilation (see [*Komen et al.*, 1994]).

In our intercomparison of SAR retrieved wave spectra with spectra computed by the WAM model we can validate not only the SAR wave mode data product and retrieval algorithm, but also the WAM model at a higher level of spectral detail than was previously feasible. However, in considering the full ERS-1 data set, we have necessarily had to restrict the analysis to an essentially statistical investigation. The period of our analysis extends over the three year period 1 January 1993 – 31 December 1995, for which reliable ERS-1 SWM data were available. Prior to 1 January, 1993, the SWM product was still in a process of modification.

The retrieval of ocean wave spectra from Wave Mode imagette spectra is not a simple exercise. The SAR imaging mechanism is strongly nonlinear because of the distortions induced by the wave orbital motions, the "velocity bunching mechanism" (cf. the MARSEN review in *Hasselmann et al.* [1985]). This leads, among other effects, to image smearing and to a loss of information beyond the so-called azimuthal cut-off wavenumber, corresponding typically to wavelengths shorter than about 100 – 200 m in the satellite flight direction. In addition, ocean wave spectra from satellite SAR images suffer from a basic 180° frozen-image ambiguity. Nevertheless, even with these limitations, [*Hasselmann and Hasselmann*, 1991], (referred to in the following as [HH]) were able to develop an efficient inversion algorithm enabling a reliable retrieval of ocean wave spectra from SAR imagette spectra within the computational constraints of real-time operational applications (see also [*Krogstad et al.*, 1994]). An essential prerequisite for the construction of an operationally feasible inversion algorithm was the derivation by [HH] of a closed nonlinear integral transform describing the mapping of ocean wave spectra into SAR spectra. It contains an exponential cut-off factor $\exp[-k_x^2\xi^2]$ that describes the azimuthal fall-off of the image spectrum beyond an azimuthal cut-off wavenumber k_x, where $\xi = v \cdot R/U$ is the rms azimuthal displacement, given by the product of the rms orbital (range) velocity v and the range-to-platform velocity ratio $\beta = R/U$. To overcome the 180° directional ambiguity and to supplement the missing SAR information beyond the azimuthal cut-off, a first guess wave spectrum is required as input to the retrieval algorithm. The imaging theory and nonlinear mapping relation have been verified in numerous studies (an overview is given in

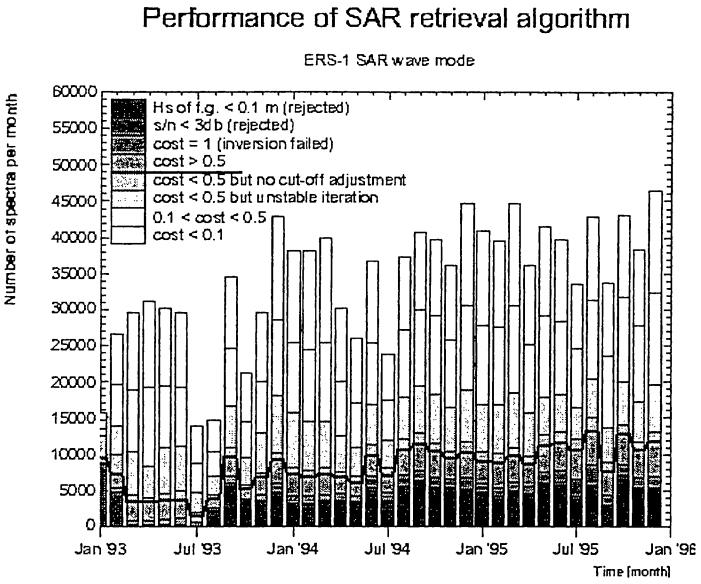

Heimbach et al. [1997], referred to in the following as [H3]). A first evaluation of this algorithm was performed by *Brüning et al.* [1994]. An improved algorithm in which the input spectrum is iteratively modified with the aid of a spectral partitioning scheme such that asymptotically only the truly missing information is carried over from the first guess spectrum has recently been proposed by [*Hasselmann et al.*,1996], (referred to in the following as [HBHH]). Furthermore, the limitation imposed by the azimuthal smearing is partially overcome in [HBHH] by including an explicit penality term for errors in the azimuthal cut-off in the cost function. The retrieval algorithm descibed in [HBHH] has been used in this study.

The WAM model plays a central role in our analysis (for a description of the present cycle 4 see [*WAMDI Group*, 1988] and [*Komen et al.*, 1994]). The model spectra were computed with the ECMWF operational wave forecast model WAM cycle 4 every 6 hours on a global 3° × 3° (since July 1994: 1.5.° × 1.5°) latitude-longitude grid. As wind forcing we used the ECMWF analyzed wind field $\mathbf{u_{10}}$ at 10m height. The WAM spectra were used to provide the first guess for the wave spectral retrievals, and we use the WAM model predictions again in intercomparing the modelled and retrieved wave spectra. This approach is not as circular as this may appear, since it has been demonstrated in [HBHH] that the improved retrieval algorithm used here, in which the first-guess input spectrum is iteratively modified, is insensitive to the initial input spectrum. The first guess information is used only to remove the 180° ambiguity and augment the retrieved spectrum beyond the azimuthal cut-off.

2. RETRIEVAL ASSESSMENT

3 year set of ERS-1 SWM data between January 3 and December 1995 comprises a total of some nillion wave spectra with an average daily output 100 spectra.

retrieval process incorporated two quality tests: .ta quality test for the input SWM data, and a .bility test for the retrieval. The input SWM data rejected if the signal-to-noise ratio of the image trum (defined as the ratio of the spectral peak to clutter noise background) was less than 3 db or e first guess wave height was below 0.1 m. The eved spectra were discarded as unreliable if the function was not reduced to less than half of its al value.

ıre 1 shows that with the beginning of the quasi -time distribution of the fast delivery product .P) in February 1993 maximally 2 % of the data showed low signal-to-noise ratios. Another 10% of the data were rejected because the first guess wave height was too low ($H_s < 0.1$ m).

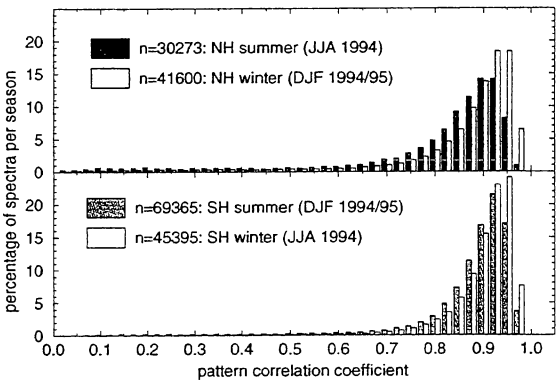

Figure 2: Distribution of pattern correlation between simulated and observed SAR spectra

For roughly 85 % of the remaining data, the retrieval algorithm achieved an acceptable performance, with cost function reductions to less than 0.5 of the initial value, while for one third a reduction factor of less than 0.1 was achieved. Spectra with a cost function reduction factor lower than 0.5 for which the azimuthal clutter cut-off adjustment or the convergence of the iterative inversion procedure was poor were nevertheless retained in the subsequent analysis, as their fidelity, (i.e. their ability to reproduce the observed SAR spectra), was generally still acceptable. The remaining 15% inversions for which the ratio of the final to initial cost could not be reduced below 0.5 generally exhibited relatively low pattern correlations between the simulated and observed SAR spectral and were discarded from the further analysis.

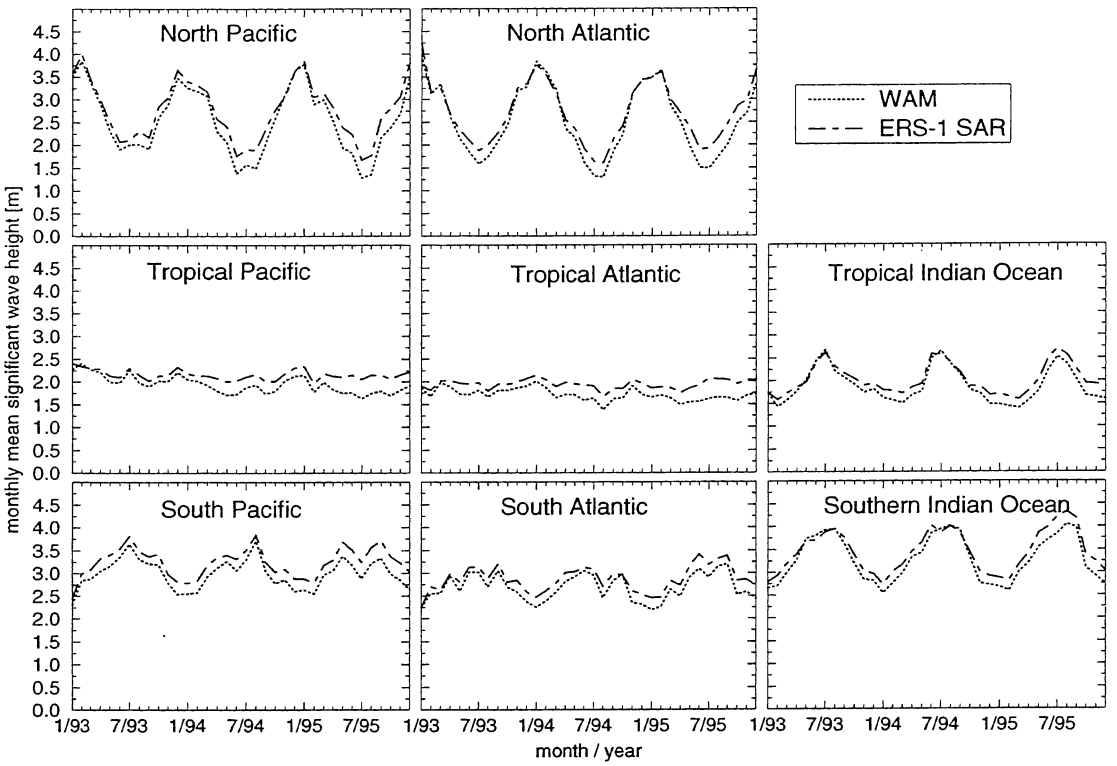

Figure 3: Time series of monthly mean significant wave heights for WAM and ERS-1 SWM.

The retrieval fidelity is represented in Figure 2 in terms of the distributions of the pattern correlation coefficients for the simulated and observed SAR spectra for the summer 1994 and winter 1994/95 seasons in the Northern and Southern Hemisphere. All distributions show a rather narrow peak around 0.9, indicating that for the major part of the data successful retrievals of high fidelity were achieved. The winter distributions in both hemispheres appear to be peaked towards slightly higher correlations than the summer distributions, suggesting that the retrieval performance is generally higher for high sea states (as may be expected from the generally higher signal-to-noise ratios for higher sea states).

An assessment of the impact of the iteration of the input spectrum revealed that for about 92 % of the retrievals the iteration yielded an improvement, 75% showing a further improvement for more than one iteration (see [H3]). The largest impact on the retrieval is found in performing the first iteration $M = 1$, suggesting that at least one iteration should be carried out. Two iterations may represent an acceptable trade-off of retrieval improvement against computing time, the additional improvements beyond $M = 2$ tending to be rather small.

3. STATISTICAL INTERCOMPARISONS

Global and regional intercomparisons between the collocated spectral wave parameters retrieved from ERS-1 SWM spectra and computed with the WAM model were carried out for the 3 year period 1. January 1993 - 31. December 1995. The collocation was performed using the nearest model gridpoint and nearest six hourly model synoptic time to the observation location and time.

3.1. Time series of significant wave heights

Figure 3 compares the time series of monthly mean significant wave height in different regions of the Atlantic, Pacific and Indian Ocean retrieved from ERS-1 SWM (dashed curve) and computed by the WAM (solid curve). The overall agreement between modelled and retrieved wave heights is satisfactory. However, a small but systematic underestimation of H_s by the WAM relative to the ERS-1 SWM data is seen. The bias is more pronounced for low sea state summer conditions. A different behaviour for different ocean basins is apparent.

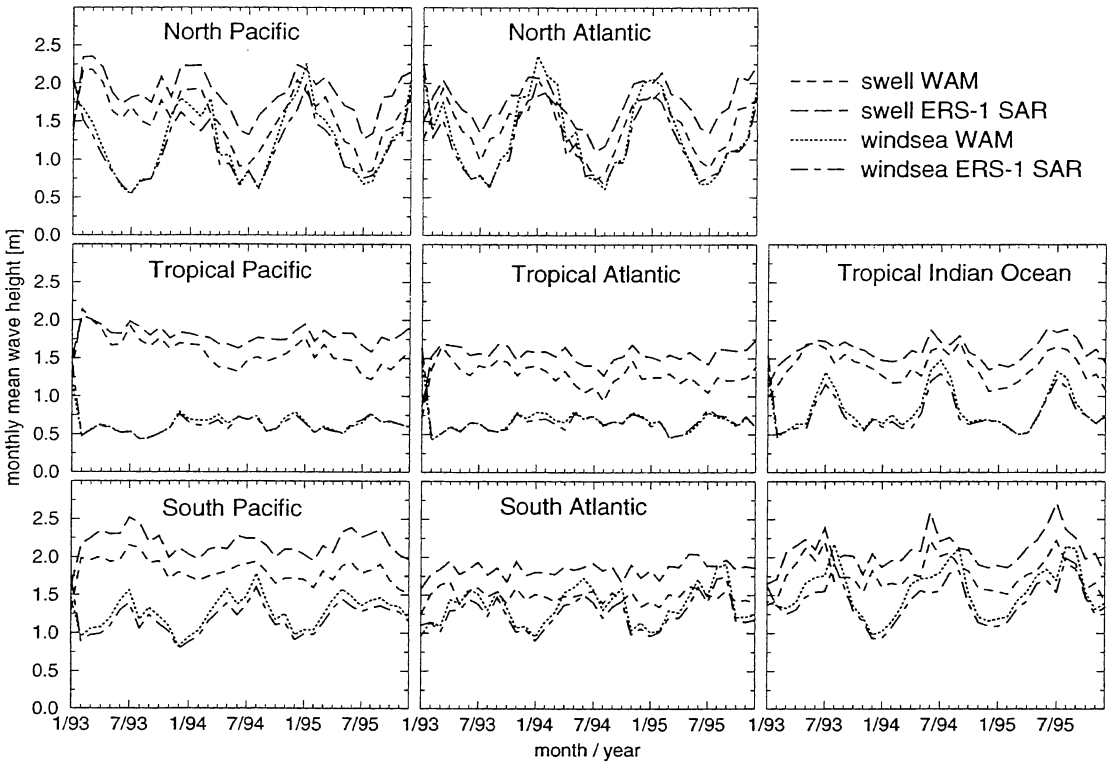

Figure 4: Time series of monthly mean windsea and swell wave heights for WAM and ERS-1 SWM.

3.2. Time series of windsea and swell wave heights

A more detailed intercomparison of modelled and retrieved wave spectra can be obtained by partitioning the spectra into wave systems. For the present analysis we have classed as windsea category young and old windsea systems (as defined in [HBHH]), while swell refers to "pure" swell. Mixed windsea-swell systems are not included in either category and are also not presented as a separate wave system class, since their contribution to the total wave energy is small.

The time series of the monthly mean swell wave heights H_{sw} (defined as the significant wave height corresponding to the total swell energy summed over all swell systems) are shown in Figure 4 for the modelled (dashed curves) and retrieved (long-dashed curves) in different basins of the Atlantic, Pacific and Indian Ocean. Also shown are the simulated and observed monthly mean windsea wave heights H_{ws} (dotted and dot-dashed curves, respectively). The general agreement between model and observation and the distinctive annual cycles are again confirmed.

However, a discrimination is now possible with respect to the small systematic deviations noted earlier between the simulated and observed total wave heights. Whereas the WAM windsea tends to be slightly overpredicted by about 10 % relative to the retrieved data, with larger relative deviations for high sea states corresponding to winter conditions, the swell wave heights are systematically underestimated by about 20 to 30 %. As the magnitudes of the windsea and swell wave heights are of the same order, the different features of the windsea and swell biases cannot be explained simply by a dependence on wave height, but must be attributed to the different spectral and dynamical properties of windsea and swell. We have considered three possible causes for the differences:

1. Results from data assimilation exercises suggest that in certain areas of the Atlantic and Pacific the ECMWF analysed wind fields produce too strong winds and thus too strong windseas (see references in [*Bauer et al.*, 1997]). However, if this were the only error, an overestimation of the windsea would necessarily lead also to an overestimation of the swell emerging from the storm, which is not found.

2. The combination of an overestimation of the windsea together with an underestimation of swell suggests a possible error in the balance between windsea and swell dissipation.

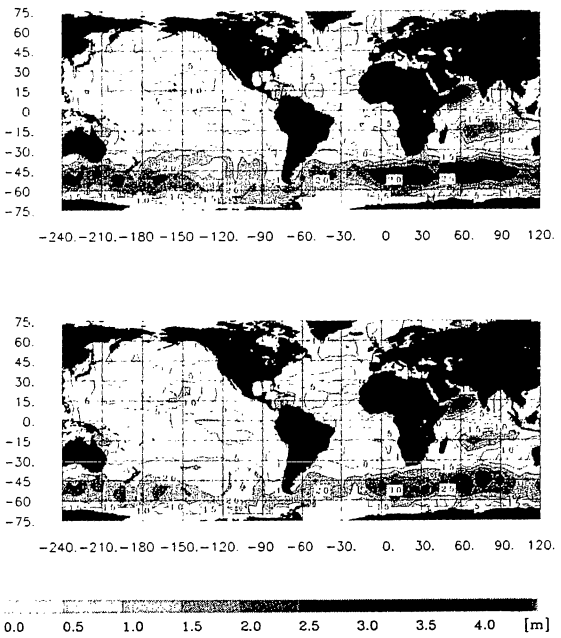

Figure 5: Global distribution of WAM (top) and SWM (bottom) seasonal mean windsea wave heights during JJA 1994.

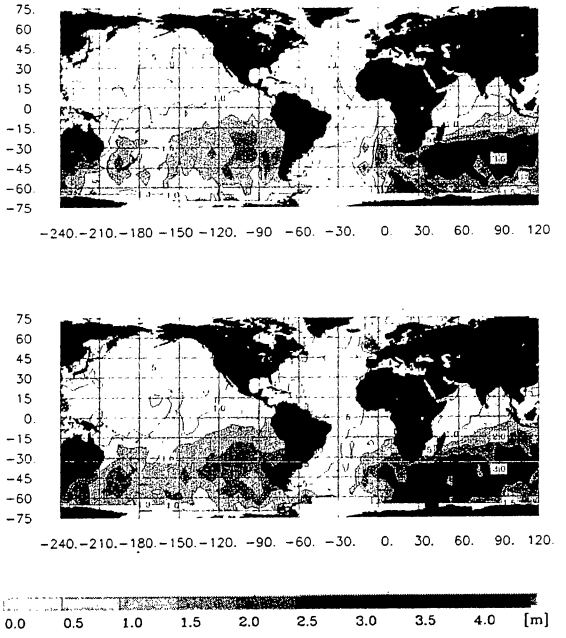

Figure 6: Same as Figure 5 but for individual swell components of largest wavelength exceeding 250m.

3. The transition regime between windsea and swell in the area close to but outside the immediate wind generation region, where the wind forcing has already decreased but the nonlinear interactions are still important, plays a critical role in determining the ratio of windsea to swell energy (see e.g. [*Young et al.*, 1987]). It is conceivable that the strongly simplified discrete interaction parametrization of the nonlinear energy transfer is inadequate for a proper representation of this process.

Numerical errors associated with the propagation scheme employed in the WAM model ([*WAMDI Group*, 1988]) can be excluded because the propagation scheme is energy conserving.

We regard the second candidate of a too strong damping for low frequency swell as the most likely explanation for the negative swell bias (for a more detailed discussion see [H3]).

Another possible source of error is indirect errors introduced by altimeter data into the operational WAM model. Since August 1993 ERS-1 altimeter wave height data have been assimilated by ECMWF into the WAM model using an optimal interpolation scheme, thereby influencing the first guess wave field through the analysis six hours earlier. However, an investigation of altimeter wave heights suggests that the impact on the first guess data available for the present study is probably rather limited (see the discussion in [H3]). We are therefore reasonably confident that, although our model data are undoubtedly affected by the assimilation of altimeter data, the dynamical aspects are at least still apparent in the data set.

3.3. Seasonal intercomparison of modelled and retrieved windsea and swell systems

Further insight can be gained by looking at regionally stratified data as a function of season. As example we show global distributions of all collocated WAM and SAR wave data – subdivided again into windsea and swell – for austral winter JJA 1994.

Windsea wave heights: Figure 5a,b shows the distributions for the WAM and SAR-retrieved windsea wave heights, respectively. They reflect the seasonal properties of the atmospheric circulation. The seasonal maps of wave heights confirm the previous findings of a generally overestimated windsea by the WAM relative to the SWM retrievals. The effect is strongest in high sea states occuring in mid-latitudes during winter. However, the modelled windsea is slightly underestimated in the trade wind regions.

Swell wave heights: For a clearer insight into the nature of the differences between the modelled and retrieved wave spectra, it is helpful to stratify the partitioned swell systems with respect to wavelength as well as direction. Figure 6a,b shows the global distributions of mean wave height for the same period

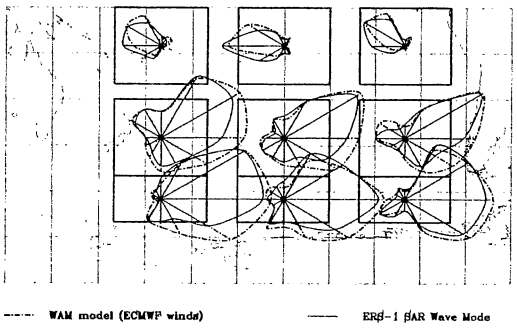

Figure 7: Seasonal mean directional windsea wave height distribution during JJA 1994 in 9 regions of the South Pacific.

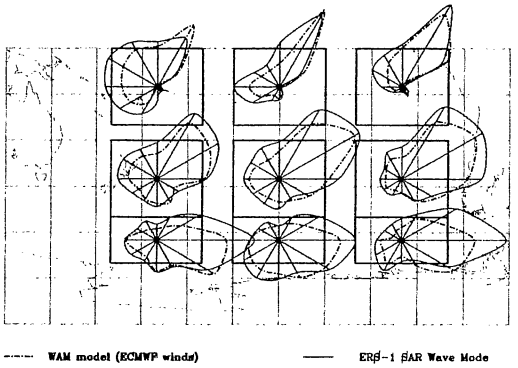

Figure 8: Same as Figure 7 but for swell.

JJA 1994 but for individual wave systems representing the longest wavelength swell with wavelength of at least 250 m. Consistent with our general findings for swell, the SWM-derived wave heights for these swell systems are again higher than the WAM wave heights. The patterns are seen to be very similar to the maps of mean swell wavelengths (see [H3]). One can thereby readily identify the main areas into which the long wavelength swell is radiated from the mid-latitude source regions.

3.4. Regional analysis for the South Pacific Ocean

As an example illustrating the detailed spectral, directional and regional information contained in the ERS-1 SWM data, we present in Figures 7 and 8 the retrieved and modelled "directional wave roses" representing the energy-weighted distributions of the wave propagation directions for windsea and swell, respectively, during JJA 1994 for nine regions in the South Pacific. The wave roses were computed as the square root of the mean energy for each 30° angular sector.

Windsea: The general zonal wind characteristics are reproduced by both the modelled and retrieved data, as well as significant deviations from the mean wind directions appearing as side lobes in the directional distributions. The WAM model overestimates mainly the E and SE travelling components, suggesting again that the model errors must be attributed at least in part to wind field errors.

Swell: The directional distributions of swell in the tropical latitudinal band between 0° and 30° S are determined by the easterly trades, producing a broad westward propagating swell sector, and the mid-latitude westerlies. The dependence on fetch leads to an increase of the trade wind swell from East to West, while the southeast travelling waves from the midlatitude westerlies to the South increase from West to East. The WAM model tends to underestimate particularly the trade wind swell components. In the latitudinal band south of 30° S, the swell is dominated by the mid-latitude westerlies, and the distributions become more isotropic, reflecting the cyclonic character of the generating storms. With a few exceptions, the WAM model underestimates the swell in all directions.

4. THE RMS ORBITAL VELOCITY

As pointed out above, a basic limitation of SAR ocean wave images is the azimuthal cut-off of the image spectrum caused by the nonlinear velocity bunching mechanism [HH], [HBHH]. The cut-off normally lies within the windsea part of the spectrum and suppresses the direct spectral information provided by the SAR on short to moderate wavelength waves with significant components of propagation in the azimuthal direction. However, the azimuthal cut-off wavenumber also provides a direct measure of an important integral parameter of the wave field: the rms orbital velocity component in the range direction. This information is used in the retrieval algorithm to adjust the rms orbital velocity to reproduce the observed cut-off, thereby partially replacing the missing direct spectral information at high wavenumbers.

The retrieval algorithm was generally successful in adjusting the simulated to the observed cut-off parameter (see [H3]). A global map of the mean azimuthal cut-off wavelength λ_c for DJF 1995/96 is shown in Figure 9. High cut-off wavelengths corresponding to high rms orbital velocities are found, as expected, in the regions of high winds in mid-latitudes. In addition, pronounced fetch effects are seen. However, no simple relationship between λ_c and u_{10} was found.

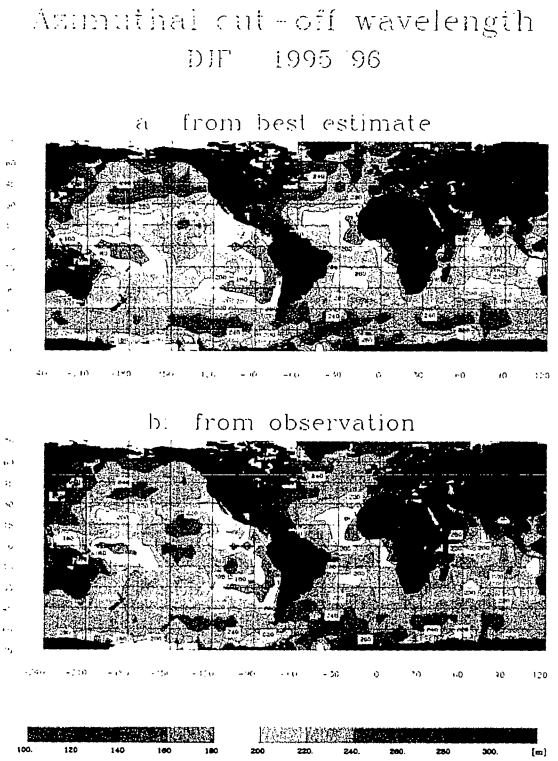

Figure 9: Global distribution of the seasonal mean azimuthal cut-off wavelength for DJF 1995/96.

5. CONCLUSIONS

In the first part of this paper we have carried out an assessment of the ERS-1 SWM data quality and the performance (fidelity) of the ocean wave spectral retrieval algorithm of [HBHH] over the three year period January 1993-December 1995 for which reliable SWM data are available. Approximately 75% of the available SWM data yielded successful retrievals.

In the statistical investigations in the second part of the paper, the SWM retrieved data were analyzed together with the corresponding data computed with the ECMWF WAM model. The data were subdivided into windsea and swell constituents, and were presented in the form of time series for different ocean basins, global maps for different seasons, and polar "wave rose" plots of directional energy distributions. In addition, results were presented for the cut-off wavelengths of the SWM spectra.

A quantitative assessment of the dynamical effects identified by our statistical approach is made difficult by the continual assimilation of observed altimeter data in the ECMWF operational model. This attenuates systematic model errors, for example in swell propagation. However, the statistical analyses nevertheless enabled the identification of a number of discrepancies between the two data sets, pointing to various features and possible shortcomings of the WAM model or the forcing wind fields which require closer investigation.

REFERENCES

Bauer, E., S. Hasselmann, P. Lionello and K. Hasselmann, 1997: Comparison of assimilation results from an optimal interpolation and the Green's function method using ERS-1 SAR wave mode spectra. *this issue.*

Brüning, C., S. Hasselmann, K. Hasselmann, S. Lehner, T. Gerling, First evaluation of ERS-1 synthetic aperture radar wave mode data. *Global Atmos. Ocean System* **2**, 61-98, 1994.

Hasselmann, K., R.K. Raney, W.J. Plant, W. Alpers, R.A. Shuchman, D.R. Lyzenga, C.L. Rufenach and M.J. Tucker, 1985: Theory of synthetic aperture radar ocean imaging. A MARSEN view. *J. Geophys. Res.* **C90**, 4659-4686.

Hasselmann, K. and S.Hasselmann [HH], 1991: On the nonlinear mapping of an ocean wave spectrum into a synthetic aperture radar image spectrum and its inversion. *J. Geophys. Res.* **C96**, 10713-10729.

Hasselmann, S., C. Brüning, K. Hasselmann and P. Heimbach [HBHH], 1996: An improved algorithm for the retrieval of ocean wave spectra from SAR image spectra. *J. Geoph. Res.* **C101**, 16615-16629.

Heimbach, P., S. Hasselmann and K. Hasselmann [H3], 1997: Statistical analysis and intercomparison with WAM model data of three years of global ERS-1 SAR wave Mode Spectral retrievals. Submitted to *J. Geophys. Res.*

G.J. Komen, L. Cavaleri, M. Donelan, K. Hasselmann, S. Hasselmann and P.A.E.M. Janssen, 1994: Dynamics and modelling of ocean waves. Cambridge University Press, Cambridge (UK), 1994, 560 pp.

Krogstad, H.E., O. Samset and P.W. Vachon, 1994: Generalization of the non-linear ocean-SAR transform and a simplified SAR inversion algorithm. *Atmosphere-Ocean* **32**, 61-82.

Young, I.R., S. Hasselmann and K. Hasselmann, 1987: Computations of the response of a wavespectrum to a sudden change in wind direction. *J. Phys. Oceanogr.* **17**, 1317-1338.

WAMDI Group (Hasselmann, K. et al.), 1988: The WAM model - a third generation ocean wave prediction model. *J. Phys. Oceanogr.* **18**, 1775-1810.